AC Magnetic Susceptibility of a Thin Film of Permalloy

Isaiah Gray

Submitted under the supervision of Dan Dahlberg to the University Honors Program at the University of Minnesota-Twin Cities in partial fulfillment of the requirements for the degree of Bachelor of Science, summa cum laude, in Physics.

May, 2014

Acknowledgements

I would like to thank my labmates, Dan Endean, Bern Youngblood, and Barry Costanzi for helpful suggestions throughout the experiment and for wire bonding. I would also like to thank Professor Dan Dahlberg for the idea for the experiment and invaluable discussion of the physics involved.

Abstract

Measurements of noise in magnetic thin films have variously reported $1/f$ noise, white noise, and random telegraph noise. The $1/f$ noise experiments claim magnetic noise by relating the magnetic noise to the susceptibility with use of the fluctuation-dissipation theorem. However, neither the linearity of the susceptibility necessary for application of fluctuation-dissipation nor the frequency dependence of susceptibility was explored. To investigate more fully the frequency dependence and linearity of the magnetic susceptibility of a magnetic film, we measured the AC susceptibility of a 100 nm thick film of permalloy as a function of the magnitude H_{AC} and frequency f of an applied AC magnetic field over the full hysteresis loop of the films, i.e., the measurements were performed while slowly varying an applied DC magnetic field, H_{DC}. The AC frequency range was from 20 Hz to 5 kHz while the AC field range was between 0.2 G and 1 G. At $H_{DC} = 0$ the response of the system was measured as a function of H_{AC} at 200 Hz. It was found to be nonlinear but became reasonably close to linear for $H_{AC} < 1G$ - the coercive field was approximately 15 G. The in-phase and out-of-phase components approximately follow power laws with frequency, with exponents 0.69 and -0.2. The behavior of the out-of-phase component is roughly consistent with previously measured white magnetic noise and a simple harmonic oscillator model, but the in-phase component does not follow the prediction of this model.

Contents

List of Figures

Chapter 1

Introduction

Microscopic magnetic systems, especially thin film stacks such as tunnel junctions, are extensively used for magnetic field sensors and random access memory devices [1]. Although critical to the engineering process, it is arguable that magnetization dynamics on small length scales remain poorly understood [2]. In addition, magnetic noise - thermally driven fluctuations of the magnetization - is important from a physics perspective as it provides information about the dynamics of the system in thermal equilibrium, without perturbing the system. In principle, magnetic noise could be determined by measuring magnetization as a function of time, but directly measuring magnetization in a microscopic system is experimentally difficult and often requires specialized equipment [3]. In practice, noise in microscopic magnetic systems is often probed by measuring the resistance fluctuations associated with giant magnetoresistance, relating the magnetization to the resistance of the sample [4]. Several groups have performed noise measurements in multilayer tunnel junctions using giant magnetoresistance and find that the power spectral density, which measures the magnitude of the Fourier component of the noise as a function of frequency [5], the noise varies inversely with the probing frequency [6], [2]. Other groups performing measurements in similar systems report white noise, or a frequency-independent power spectral density [7].

The lack of consensus on the functional form of magnetic noise in thin film systems is more problematic as recent studies cast doubt on the accuracy of the previous reports of observations of $1/f$ noise in many of the studies [8]. The magnetic aftereffect is associated with the finite response time of a magnetic system when the field is adjusted. Plotting this time-dependent response in the frequency domain yields a $1/f$ spectrum similar to observed $1/f$ spectra, so more information is needed to distinguish time-dependent effects from true magnetic $1/f$ noise.

A powerful tool to interpret observations of magnetic noise is the fluctuation-dissipation

(FD) theorem [9], which relates the noise spectra of an observable of a system at thermal equilibrium to the susceptibility, or response of the system to small perturbations. This has been the approach taken by many researchers in their explorations of noise. In principle, to apply the theorem it is necessary to know the response in the limit of vanishingly small perturbations. Experimentally, the perturbations must at least be small enough to observe linear response, so that the data can be extrapolated to estimate zero-perturbation response. A ferromagnet is a strongly nonlinear system, however, exhibiting hysteresis for oscillating fields [10], so it is not clear that FD applies in this situation. Assuming a linear response, since noise is measured as a function of frequency, the susceptibility must also be measured as a function of frequency. There are many studies of AC magnetic susceptibility as a function of DC field amplitude in the literature [2] [6], but the frequency dependence over a large enough range to effectively apply the FD theorem has been largely unexplored. The goal of the present experiment was two-fold: to test the experimental applicability of the fluctuation-dissipation theorem by measuring the response of a magnetic thin film to small AC applied fields, and to measure the frequency dependence of AC magnetic susceptibility.

Chapter 2

Background

2.1 Magnetization

A material placed in a magnetic field H will acquire a magnetization M [11], defined to be the net magnetic dipole moment per unit volume. In a paramagnet or a ferromagnet above the Curie temperature the response is proportional to the applied field, and the constant of proportionality is called the susceptibility, χ:

$$\mathbf{M} = \chi \mathbf{H} \tag{2.1}$$

If **M** and **H** are collinear, χ is simply a scalar. The response of a ferromagnet to an applied field is more complex. As shown in Fig 2.1, **M** is not linear with **H** nor even a single-valued function of **H**. The magnetization at a given field depends on the previous history of the field as well as its present value [10].

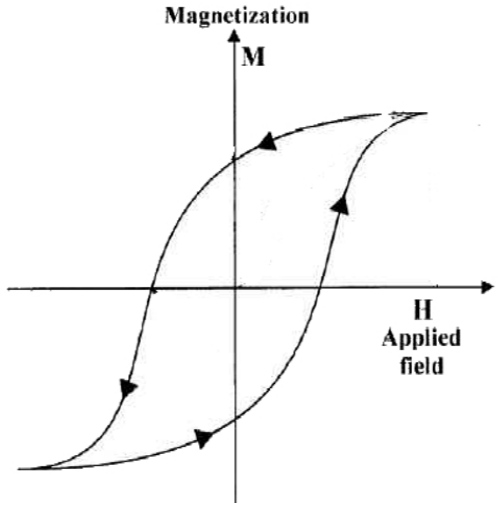

Figure 2.1: An example of a hysteresis loop in a ferromagnet. The arrows represent the direction of field sweep, from negative to positive and back to negative.

Since **M** is not linear with **H**, the susceptibility is now DC field dependent and we can define the field-dependent χ as

$$\chi = \frac{dM}{dH}. \tag{2.2}$$

A ferromagnetic material in an AC magnetic field can be modeled as a damped driven harmonic oscillator for many purposes [12], giving rise to the phenomenon of ferromagnetic resonance. Just as there is a phase shift between the driving force and the displacement in a damped harmonic oscillator, there is a phase shift between the magnetization and the AC applied field. If the driving force is

$$H = H_0 \sin \omega t, \tag{2.3}$$

the response is

$$M = M_0 \sin(\omega t + \phi). \tag{2.4}$$

Expanding out the sine,

$$M = M_0 \cos\phi \sin \omega t + M_0 \sin\phi \cos \omega t. \tag{2.5}$$

The response is now seen to have an in-phase component, $M_0 \cos\phi$, and an out-of-phase component $M_0 \sin\phi$. Alternatively, we may define the susceptibility as a complex number:

$$\chi = \chi' + i\chi'', \tag{2.6}$$

where the real part χ' is the in-phase component and the imaginary part χ'' is the out-of-phase component. The phase angle can then be written:

$$\phi = \tan^{-1} \frac{\chi'}{\chi''}. \tag{2.7}$$

2.2 Magnetic Noise

At any non-zero temperature, the direction of spin of the electrons in a ferromagnet, and therefore the magnetization, will fluctuate slightly around a mean value. These fluctuations can be experimentally measured in microscopic thin films, where they are called magnetic noise to distinguish from other sources of noise. An example of generic white noise measured with arbitrary units in the time domain is shown in Fig 2.2 below.

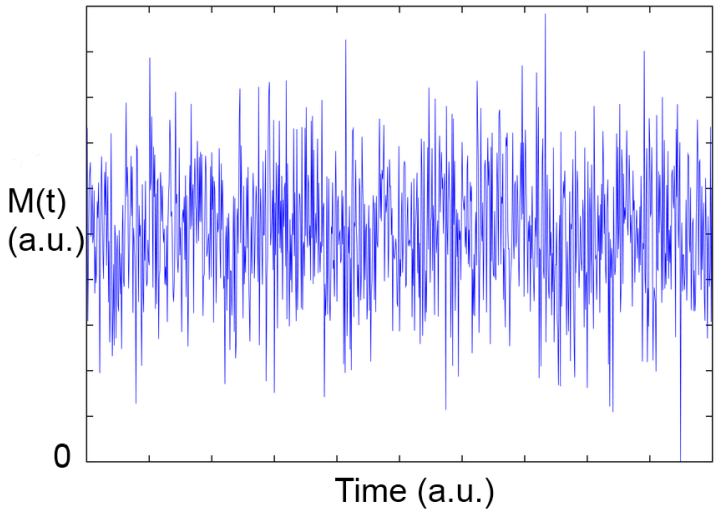

Figure 2.2: An example of white noise plotted in the time domain.

It is more useful, however, to perform a Fourier transform on the time domain signal and consider noise in the frequency domain, so that

$$\hat{M}(\omega) = \int_{-\infty}^{t} M(t')e^{-i\omega t'}dt'. \tag{2.8}$$

We define the power spectral density [5] as

$$S(\omega) = \|\hat{M}(\omega)\|^2. \tag{2.9}$$

$S(\omega)$ is a measure of the amplitude of the various frequencies which together comprise the noise signal and is the standard measure of noise in a system.

Several groups beginning with Parkin et. al. [6] have performed noise experiments in thin film stacks comprised of a layer of non-magnetic Cu sandwiched between layers of Co. The width of the spacer Cu layer is chosen so that at zero applied field the Co layers align antiferromagnetically, or antiparallel. In a large applied field the layers rotate with the magnetization into a parallel state, and in a smaller applied field the angle between the magnetizations fluctuates with time, resulting in magnetic noise. Noise was measured using the giant magnetoresistance effect, which relates the electrical resistance measured through the layers of the stack to the angle between the magnetizations of the two layers [2]. The power spectral density of the noise measured was found to vary inversely with frequency as shown in Fig 2.3 below.

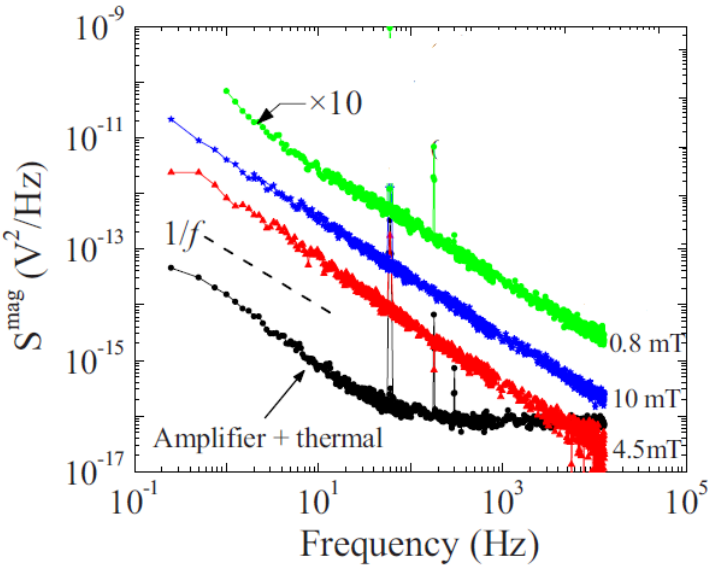

Figure 2.3: Data taken from [2]. A log-log plot of the power spectral density as a function of the probing frequency. The curve is linear with a slope of -1, showing a $1/f$ spectrum.

By contrast, Smith et al [7] have performed similar magnetoresistance measurements with GMR thin films in which the active elements were a CoFe layer whose magnetization was fixed or pinned by antiferromagnetically coupling to a layer of PtMn, and a free magnetic layer of CoFe, whose magnetization would rotate with an external field. Magnetic noise was indirectly measured through the giant magnetoresistance effect as in

Parkin's experiments but the DC fields were applied from -200 G to 200 G, as opposed to Parkin's range of 0 - 45 G. The power spectral density was found to be constant or flat with frequency as shown in Fig 2.4 below.

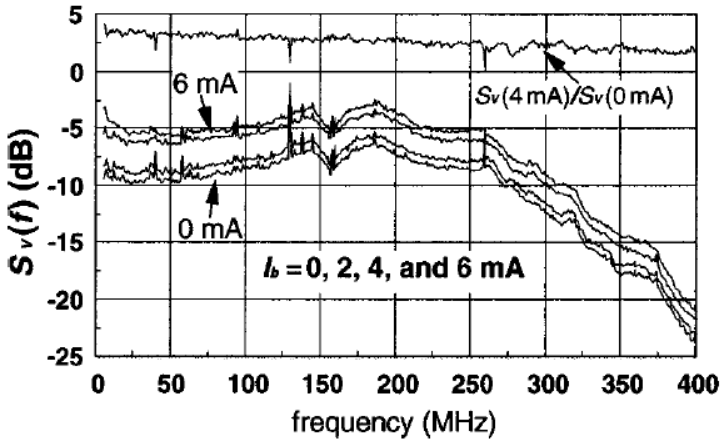

Figure 2.4: From [7]. Another noise measurement in systems similar to those in [6], but the power spectral density is approximately flat from 0 - 250 MHz, disagreeing with a $1/f$ spectrum.

Giant magnetoresistive stacks offer the advantage of a large, easily measurable signal but also the disadvantage of a complex system with potential nonmagnetic sources of noise, such as defects in the antiparallel state [6]. In addition, Guo's work [8] demonstrates that the time lag of the response when a changing field is applied can appear very similar to noise. Since noise data by itself is insufficient to determine the source of the noise, these qualitatively different results demonstrate that interpreting noise data in magnetic thin film stacks is not straightfoward. Additional information is required to distinguish between magnetic noise and other sources of noise, which in both these experiments comes from application of the fluctuation-dissipation theorem.

2.3 The Fluctuation-Dissipation Theorem

The fluctuation-dissipation (FD) theorem relates fluctuations in a dynamical variable of a system at thermal equilibrium to the response of a system to a small perturbing force [9]. In general the theorem states:

$$S(\omega) = \frac{2k_B T}{\omega}\hat{\chi}''(\omega), \tag{2.10}$$

where $\hat{\chi}''(\omega)$ is the imaginary part of the susceptibility as a function of frequency, obtained by taking the Fourier transform of $\chi''(t)$.

In a magnetic system, if the susceptibility to applied magnetic fields is known as a function of frequency, the functional form of magnetic noise at thermal equilibrium can be predicted. However, one of the conditions necessary to apply the theorem is that the response of the system be linear with the perturbing force. This condition is necessary because $\hat{\chi}''(\omega)$ is a differential quantity, and although it is not possible experimentally to measure dM with zero dH amplitude, if dM is linear with dH the data may be extrapolated to obtain $\hat{\chi}''(\omega)$. Fig 2.1 shows that a ferromagnet is inherently a non-linear system under an AC perturbation, so in principle FD cannot be applied in this case. However, one may expect that for small enough amplitudes, the response may be approximately linear as shown in Fig 2.5, and FD would be approximately valid.

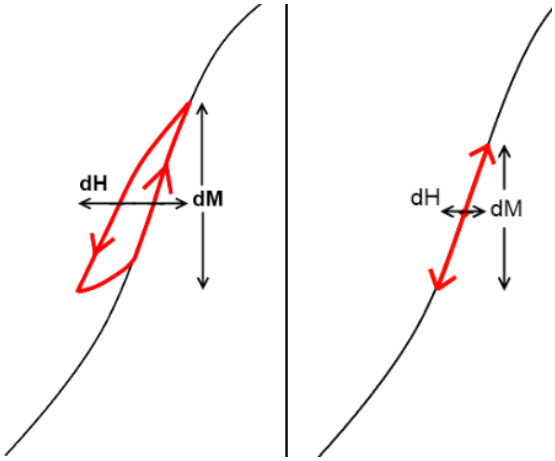

Figure 2.5: Possible responses of a ferromagnet to a small AC applied field. The left plot shows a minor hysteresis loop, exhibiting nonlinear behavior, while the right plot schematically shows a linear response.

To apply FD to understand noise in a ferromagnetic thin film, $\hat{\chi}''(H_{AC})$ must first be measured to make sure that the response is indeed linear at small amplitudes so that

FD applies. Assuming this is done, $\hat{\chi}''(\omega)$ must be measured over the same range of frequencies as $S(\omega)$ to adequately compare the two. Both the $1/f$ and the flat noise experiments use FD to interpret noise data, but neither measure $\hat{\chi}''(\omega)$ over the same range of frequencies as $S(\omega)$. Fig 2.3 from the $1/f$ experiments shows that $S(\omega)$ is measured over six orders of magnitude from 10^{-1} Hz to 10^5 Hz, but $\hat{\chi}''(\omega)$ is measured to be approximately constant over a factor of 2 in frequency around 50 Hz, and then assumed to be constant over the rest of the frequency range. The observed noise spectrum is then compared with the spectrum predicted by susceptibility measurements in Fig 2.6 below.

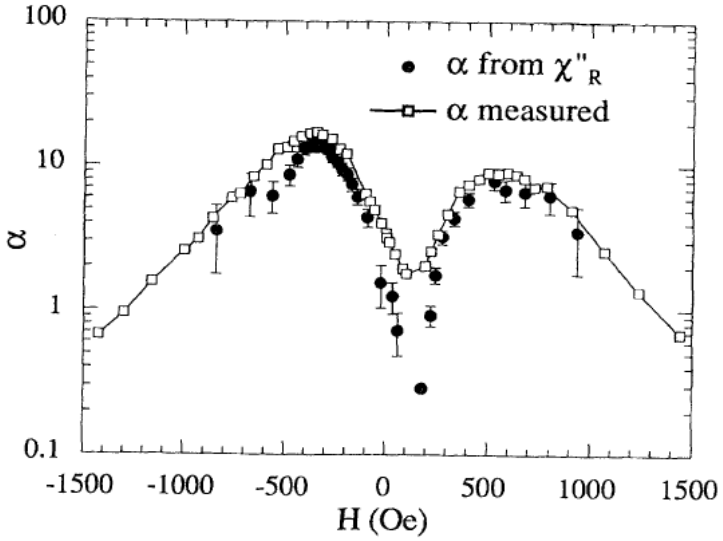

Figure 2.6: From [6]. α on the y-axis is $fS(f)$ and is called the noise parameter. The two plots compare measured noise and the noise predicted by extrapolating a constant $\chi(f)$ and applying the fluctuation-dissipation theorem. Divergence of the two is strongest at zero applied field, where χ should be most different from zero.

Measured noise data quantitatively matches a constant imaginary susceptibility at large DC fields, but the two sets diverge at zero applied field. One might expect that susceptibility would be near-constant with frequency at large DC fields, since the magnetization is trapped in a low-energy state aligned with the DC field, but it is not obvious that $\hat{\chi}''(\omega)$ would be constant at zero DC field where the magnetization is free to rotate. Indeed, the simple harmonic oscillator model described earlier predicts a non-constant $\hat{\chi}''(\omega)$. Smith et al do not measure magnetic susceptibility but estimate it

by approximating the free magnetic layer as a single-domain particle and applying the Landau-Lifshitz-Gilbert equation [7].

The present experiment attempts to solidify magnetic noise analyses by measuring $\hat{\chi}''(\omega)$ over a frequency range of 20 Hz to 5 kHz. To avoid the complexities of a multi-layer magnetic system, measurements were performed on the simplest system possible - a single magnetic thin film. Although susceptibility measurements were comparatively straightforward to interpret, the different types of magnetization measurement necessary meant that noise measurements were impractical.

Chapter 3

Experimental Setup and Methods

3.1 Sample Design

The sample was a thin film of Permalloy, an 80% Ni and 20% Fe alloy chosen for its relatively high AMR and low coercivity [13], and was about 25 μm long, 1 μm wide, and 100 nm thick. The sample was patterned with optical photolithography and deposited by sputtering onto a plain Si substrate. A schematic is shown in Fig 3.1 below.

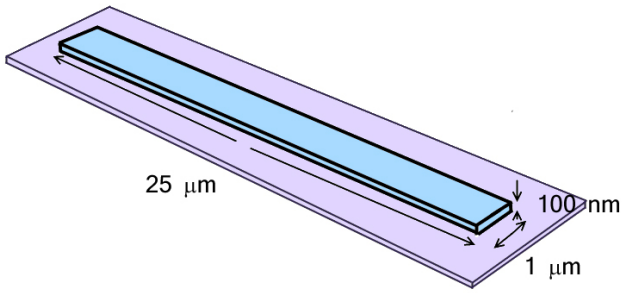

Figure 3.1: A schematic of the sample with dimensions. The purple region represents the permalloy sample, and the blue the Si substrate.

3.2 Anisotropic Magnetoresistance

Susceptibility measurements require knowledge of magnetization, a difficult quantity to directly measure in microscopic systems. However, when current is run through a magnetic sample the resistance is dependent on the relative orientation of the magnetization and the current, a phenomenon called magnetoresistance (MR) [14]. Since resistance can be measured quickly and accurately, MR is currently one of the preferred method to measure magnetization in microscopic thin films [4]. There are several types of MR - the present experiment utilized anisotropic magnetoresistance (AMR), in which the resistance of the sample is a maximum when the magnetization is collinear with the

current and a minimum when the magnetization is perpendicular to the current [15], as shown in Fig 3.2 below.

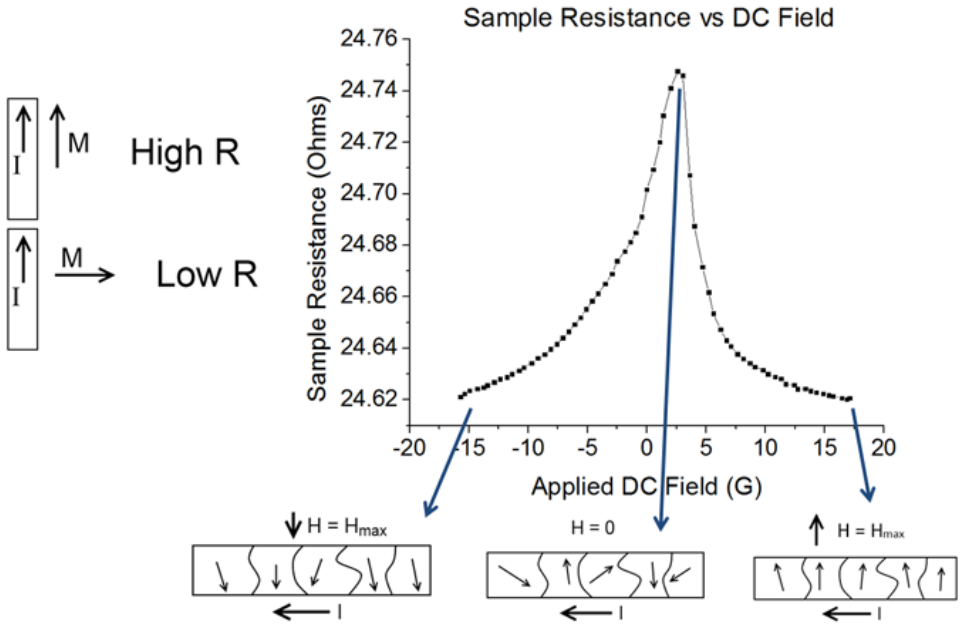

Figure 3.2: The anisotropic magnetoresistance effect in ferromagnets. The plot shows the resistance of the permalloy sample as a function of DC magnetic field applied perpendicular to the current. Since there is no field applied parallel to the current, the full magnitude of AMR is not observed.

In the present experiment, current was applied through the length of the Permalloy bar, and the magnetic field was applied perpendicular to the current. Resistance changes for full field sweeps in both directions are shown in Fig 3.2. The resistance is lowest at high fields in either direction and greatest at zero field. Since the field is not applied parallel to the current, the magnitude of the observed MR, about 0.5%, is as great as the literature value of 1.5% - 2% in permalloy [15].

The detailed mechanism of AMR, although well-understood, is not important to the present experiment and AMR should be thought of as a reliable way to relate magnetization to resistance. Quantitatively, the fractional change in resistance when current is applied perpendicular to the magnetization is given by [14]

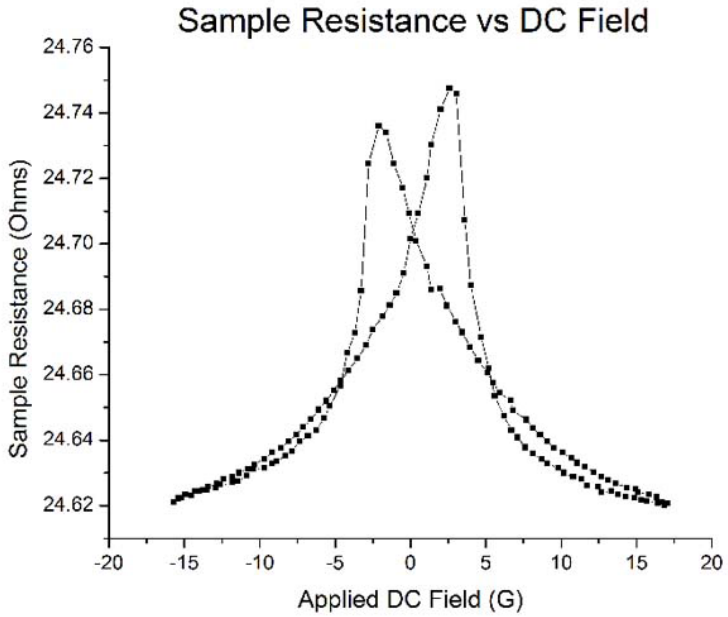

Figure 3.3: The resistance of the permalloy sample as a function of applied DC field. Since the resistance is a maximum when $M = 0$, which occurs at distinct DC fields depending on if the field were swept from positive to negative or negative to positive, two AMR peaks are observed.

$$\frac{R(H) - R(0)}{R(H)} = \beta \left(\frac{M}{R(H)} \right)^2, \tag{3.1}$$

where $R(H)$ and $R(0)$ are the measured resistances at applied fields of H and 0, respectively. Taking the derivative with respect to R,

$$\frac{dM}{dR} = \frac{R - R_0}{(R^2 - RR_0)^{3/2}} \tag{3.2}$$

Since the magnetic susceptibility $\chi_M = \frac{dM}{dH}$ and AMR resistance susceptibility $\chi_R = \frac{dR}{dH}$ are related by

$$\chi_M = \frac{dM}{dR}\chi_R, \tag{3.3}$$

the magnetic susceptibility can be written entirely in terms of measurable quantities. With the values of $R(H)$ and $R(0)$ in this experiment, $\frac{dM}{dR}$ varies by a few percent. Since χ_R varies by close to an order of magnitude, to a good approximation

$$\chi_M \propto \chi_R. \tag{3.4}$$

Measurements of χ_R will therefore be taken throughout this thesis as representative of χ_M.

3.3 Experimental Setup

A simplified diagram of the experimental setup is shown in Fig 3.4 below. A constant current of 0.93 mA was run through the length of the sample and the resistance was measured through a standard four-terminal configuration.

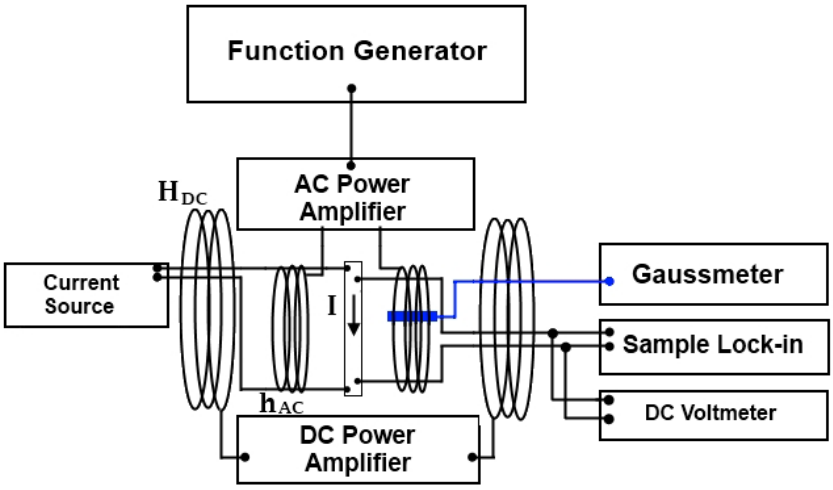

Figure 3.4: A diagram of the experimental setup. DC and AC fields were applied perpendicular to the direction of current in the sample.

The magnetization of the sample, $\mathbf{M}(\mathbf{H})$, was determined by applying a DC field and measuring resistance. Similarly, the susceptibility $\chi = \frac{dM}{dH}$ was determined by applying a small AC field dH on top of a bias field H_{DC} and measuring the amplitude

dR of the AC resistance change produced. The amplitude of the AC field, its frequency and the amplitude of the DC field were independently varied. A Stanford Research Systems DS345 function generator was used to generate the AC signal, which was then amplified by a Yamaha audio amplifier before driving the inner coils. A Kepco bipolar operational amplifier generated DC current to drive the outer coils. The magnetic field was measured with an FW Bell 5080 gauss meter inside the inner coil. The real and imaginary parts of the susceptibility were measured with a two-channel Stanford Research Systems SR530 lock-in amplifier. The collection of data was automated with a custom LabVIEW program.

The lock-in measured the magnitude of the input AC voltage signal as well as the phase of the signal relative to a reference signal, in this experiment the applied magnetic field. Although the amplitude of the field could be measured accurately with the Hall probe gaussmeter, at high frequencies the processing circuitry caused a phase shift between the actual field and the signal, so the phase difference between the resistance and the field could not be measured with the gaussmeter. However, the magnetic field was in phase with the current through the coils, so a 7.5Ω resistor was placed in series with the coils to convert the current signal into a voltage signal. The voltage across the power resistor was then amplified with a simple 741 op-amp inverting amplifier to provide a large, clean signal with no phase shifts, and then fed into the lock-in reference input as shown in Fig 3.5.

The op-amp inverting amplifier was used both to provide a clean reference signal of about 1 V at low AC fields and to avoid overloading the lock-in reference input at higher AC fields. Using an amplifier was preferable to simply using a larger resistor, since a larger resistor meant more current was necessary from the power supply. A carbon-film resistor decade box was used as the variable resistor to minimize any phase shift that might result from the finite inductance of a potentiometer. The op-amp was powered by two 9V batteries wired together.

The phase of the resistance signal relative to the applied field could be roughly measured by turning off the current through the sample and varying the magnitude of the

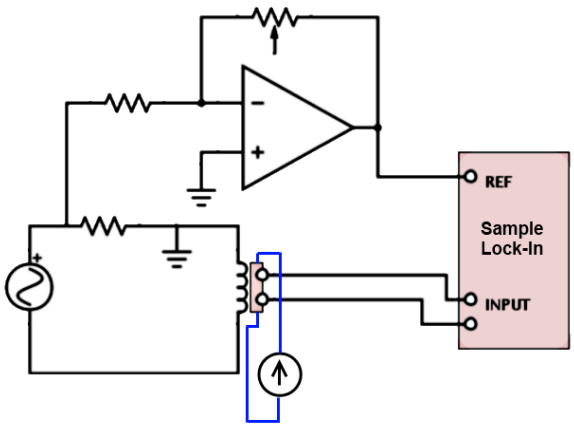

Figure 3.5: A schematic of the amplifier circuit used to accurately determine the phase of AC magnetic fields. A 741 op-amp inverting amplifier was used to amplify the voltage across the power resistor to 1 V AC signal preferred by the lock-in reference input.

AC field. With no current, there was no magnetoresistance, so one would expect zero response. However, as shown in Fig 3.6 below, the sample was attached by wire bonds to contact wires.

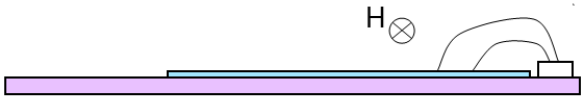

Figure 3.6: A more detailed schematic of the sample than in Fig 3.1. Indium wire-bond contacts connected the surface of the sample to a lead box, which led into BNC cables.

An alternating magnetic field through the wire bond loops produced a Faraday EMF, which produced a voltage 90 degrees out of phase with the applied field. If the reference phase was set properly, the real part was zero and the imaginary part was linear with applied amplitude as shown in Fig 3.7.

For every measurement involving an AC magnetic field, data runs were taken with and without current applied and the imaginary background was subtracted off. This background is not just an annoyance, since it could be used to check that the reference

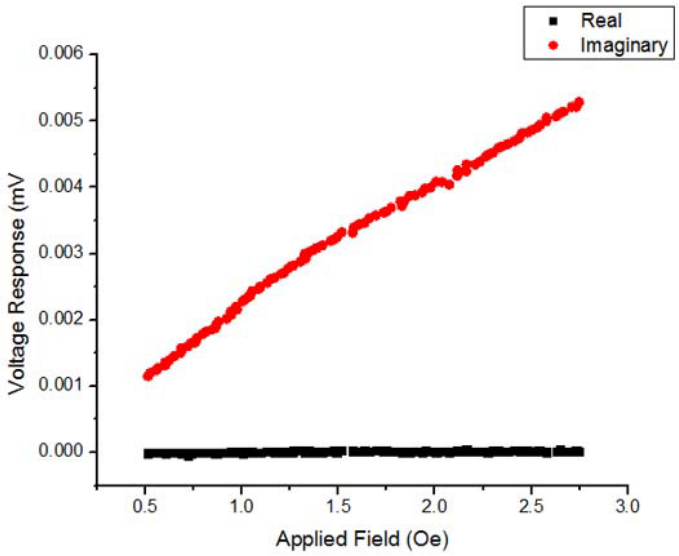

Figure 3.7: The response of the sample at zero current as a function of AC applied field, showing the linear background effect from Faraday EMF through the wire bonds. The background was used to adjust the phase of the lock-in relative to the applied field.

phase of the lock-in was set correctly. If the lock-in reference signal were out of phase with the applied field, the real component would have a non-zero slope. Using this method, a frequency-dependent shift between $-20°$ and $20°$ was found between the reference input and the applied field, despite efforts taken to ensure no phase shifts signal processing. The origin of this shift is unknown - at each measurement, the phase of the lock-in was manually adjusted to compensate.

Chapter 4

Results

4.1 Susceptibility as a function of DC Field: Testing Linear Response

To test for a linear response, the real part of the AC response of the permalloy thin film was measured as a function of AC field amplitude. Data was taken at zero DC applied field, where the magnitude of the AMR signal was a maximum. Results are shown in Fig 4.1below.

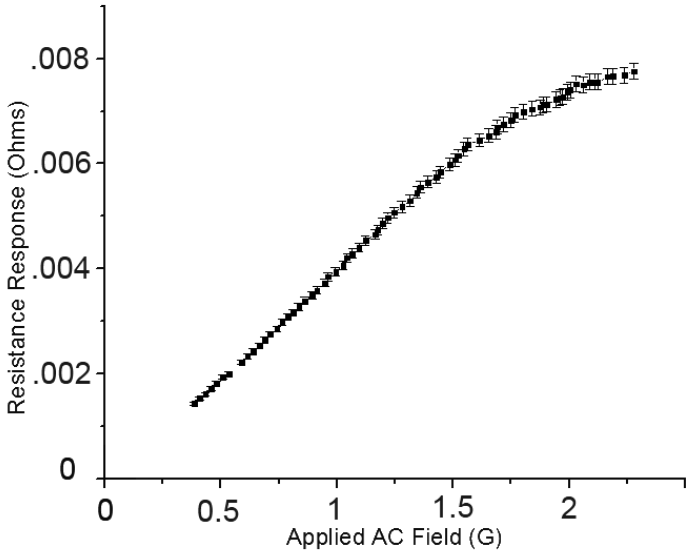

Figure 4.1: The susceptibility at 0 DC field plotted as a function of H_{AC}. At small amplitudes the response is approximately linear.

The linearity of $\chi(H_{AC})$ was estimated by performing linear fits on different regions of the curve as shown in Fig 4.2. The red curve represents a linear fit over the bottom 10 values of applied field, the green curve uses the lowest 25 values, and the blue curve

uses the lowest 40 values.

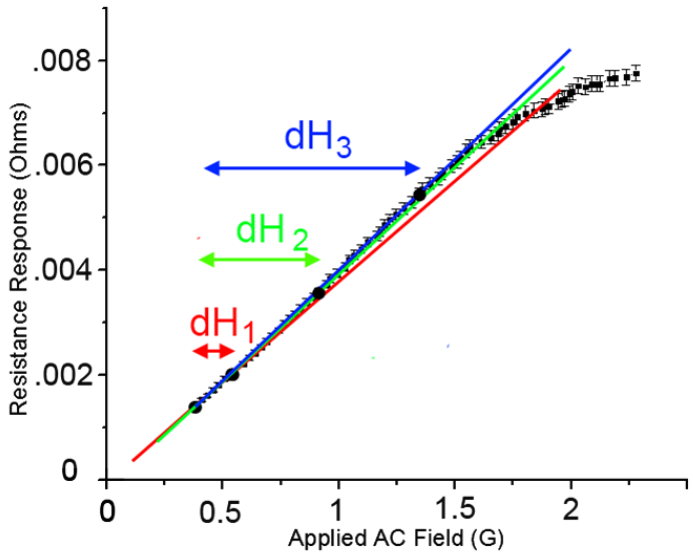

Figure 4.2: The same data as Fig 4.1 with linear fits using three different regions of χ. The red curve extrapolates from the bottom 10 data points, the green curve uses the first 25, and the blue curve uses the first 40. The slopes differ from each other by about 4%, but a least-squares weighted mean reveals that they differ from the mean slope by, respectively, 3.2σ, 2.1σ, and 2.3σ.

The slopes for the red, green, and blue curves were found to be $(3.91 \pm 0.07) \times 10^{-3}$, $(4.07 \pm 0.03 \times 10^{-3}$, and $(4.18 \pm 0.02) \times 10^{-3}$, respectively. The weighted mean, obtained by least-squares analysis, is $(4.13 \pm 0.02) \times 10^{-3}$, so the slopes obtained are, respectively, 3.2σ, 2.1σ, and 2.3σ from the mean value. Uncertainties on the data points were obtained by taking the standard deviation over several runs, but may have been underestimated. The slopes all differed from the mean by less than 5%, so it was concluded that $\chi(H_{AC})$ was approximately linear in the 0.2 G - 1 G H_{AC} range, so that the fluctuation-dissipation theorem could be applied. Measurements of $\chi(f)$ were taken within this range.

4.2 Susceptibility as a function of DC Field: Mapping out the Hysteresis Loop

In general $\chi = \chi(H_{AC}, H_{DC}, f)$, although most attention is focused where χ is greatest, around $H_{DC} = 0$. In principle H_{AC} should be as small as possible to best approximate linear response, but as H_{AC} decreased the AC signal became increasingly noisy. A balance between signal-to-noise ratio and linear response was found between $H_{AC} = 0.2G$ and $H_{AC} = 1G$. To account for the variation of χ with H_{DC}, instead of fixing H_{AC} and H_{DC} and directly varying f, H_{AC} and f were fixed, χ was measured as a function of H_{DC}, and the measurement was repeated for different frequencies. As shown in Fig 4.3, this susceptibility measurement amounts to taking the derivative of the AMR curve.

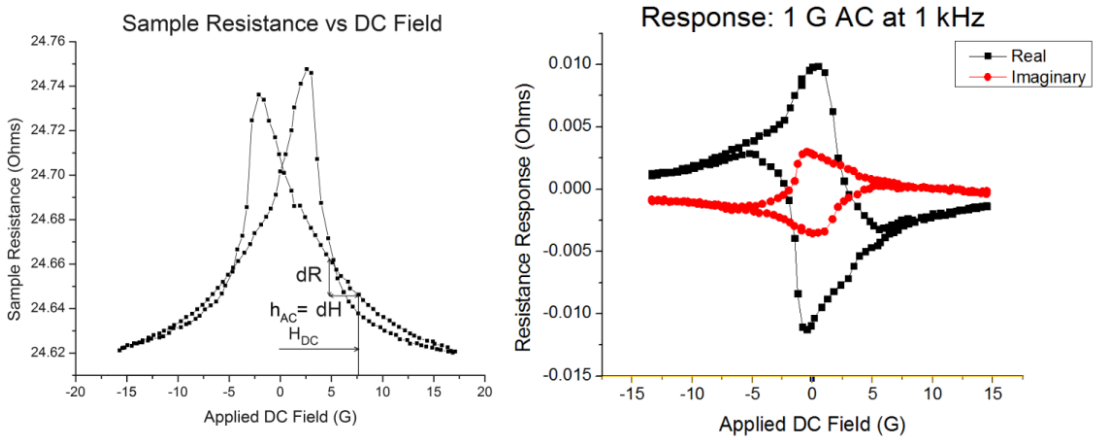

Figure 4.3: The left plot shows the AMR curve with both sweeps as shown in Fig 3.2, while the right graph plots χ as a function of H_{DC} at fixed H_{AC}, measuring the slope of the left curve at every point.

The right curve in Fig 4.3, plotting the real and imaginary parts of the susceptibility as a function of DC field using an AC field of amplitude 1 G at 1 kHz, may be interpreted as follows. At high magnitude of applied field, the susceptibility approached zero, since the thermal energy kT was small compared to the energy of alignment with the field μB and the spins could not fluctuate very much. The susceptibility was greatest when $\mathbf{M} = 0$, which occurred at two distinct values of H depending on the previous

history of the applied field. A schematic of these low and high-energy states is shown in Fig 4.4 below. χ is negative for certain fields, reflecting the fact that in performing the measurement H_{DC} was swept from a negative field (defined by the Hall probe) to a positive field and back down to negative. Tracing out the hysteresis loop, moving along a region in which the resistance decreased with applied field resulted in a negative susceptibility.

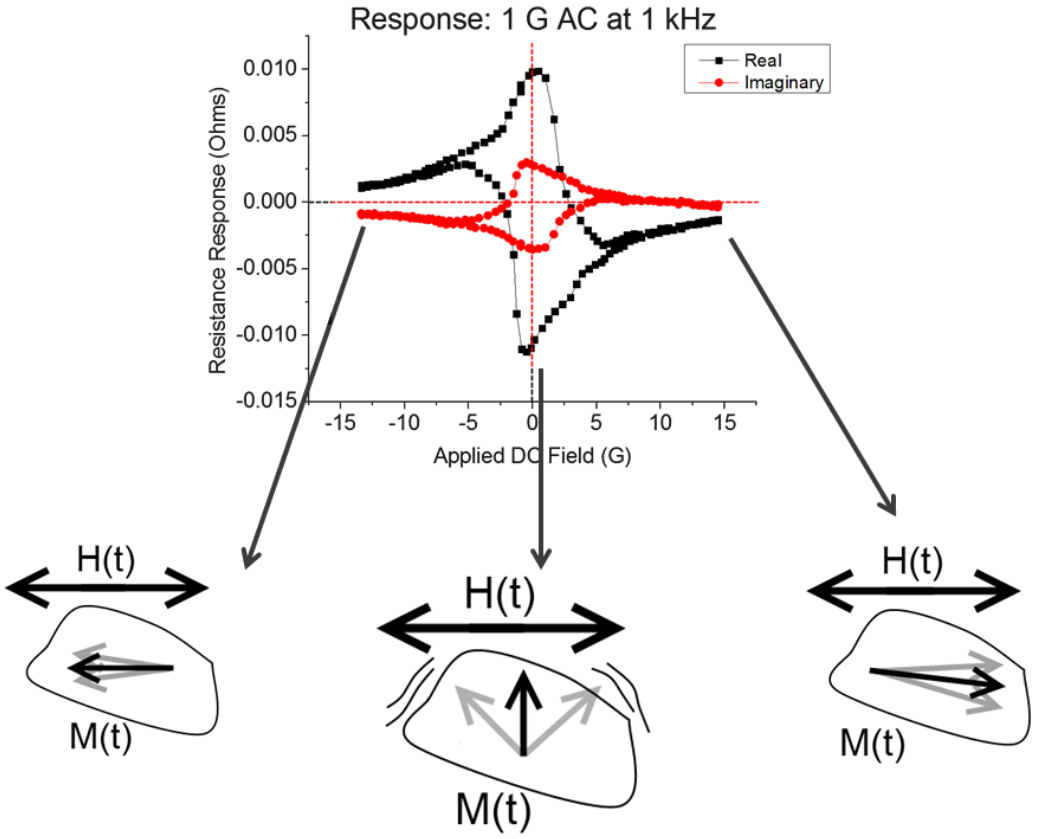

Figure 4.4: $\chi(H_{DC})$ at fixed f and H_{AC} as before. In this case, $f = 1$ kHz $H_{AC} = 1$ G peak-to-peak. At high fields, the magnetic domains align strongly with the field and do not fluctuate much, resulting in a low susceptibility. χ is a maximum when the magnetization is zero, which occurs near $H = 0$.

4.3 Susceptibility as a function of Frequency: Predicting magnetic noise

Data runs were taken at AC amplitudes of 0.2 G, 0.5 G, and 1 G AC, searching for the optimum balance between most linear response at low H_{DC} and largest measured signal at high H_{DC}. At each AC amplitude, dR was measured as a function of H_{DC} over the whole hysteresis loop at 20 Hz, 50 Hz, 100 Hz, 200 Hz, 500 Hz, 1 kHz, 2 kHz, and 5 kHz for a total of 24 data runs. Nonlinear background effects were observed at frequencies above 5 kHz. Plots of $Re(\chi(H_{DC}))$ and $Im(\chi(H_{DC}))$ taken at $H_{AC} = 0.5G$ for different frequencies are shown in Fig 4.5 and Fig 4.6 below.

The two values of H_{DC} at which the frequency dependence of χ was most interesting: $H_{DC} = 0$, where the susceptibility was greatest, and $H_{DC} = 2.5G$, where the AMR resistance was a maximum. For every H_{DC} two values of χ were measured depending on the direction of field sweep as shown in Fig 4.3, so the difference between the two was taken to be the value of χ. The reason for the large value of χ at 20 Hz is not understood, but it is common to all data sets taken. Final plots of the real and imaginary parts of χ as a function of frequency at 0 DC field are shown in Fig 4.7 and Fig 4.8 and at 2.5 G DC field in Fig 4.9 and Fig 4.10.

$\chi(f)$ at 2.5 G DC exhibits the same general trend as $\chi(f)$ at 0 G DC, except that the data appears to be noisier, especially at lower frequencies, and trends are less evident. This result is not surprising since the dR measured is about a factor of two reduced at $H_{DC} = 2.5G$ from its value at $H_{DC} = 0G$.

Returning to the fluctuation-dissipation theorem,

$$S(\omega) = \frac{2k_B T}{\omega}\hat{\chi}''(\omega), \tag{4.1}$$

if $\hat{\chi}''(\omega) \propto \omega$, $S(\omega)$ should be constant, not $1/f$, consistent with the results of [7] and the deviation at $H = 0$ found in [6].

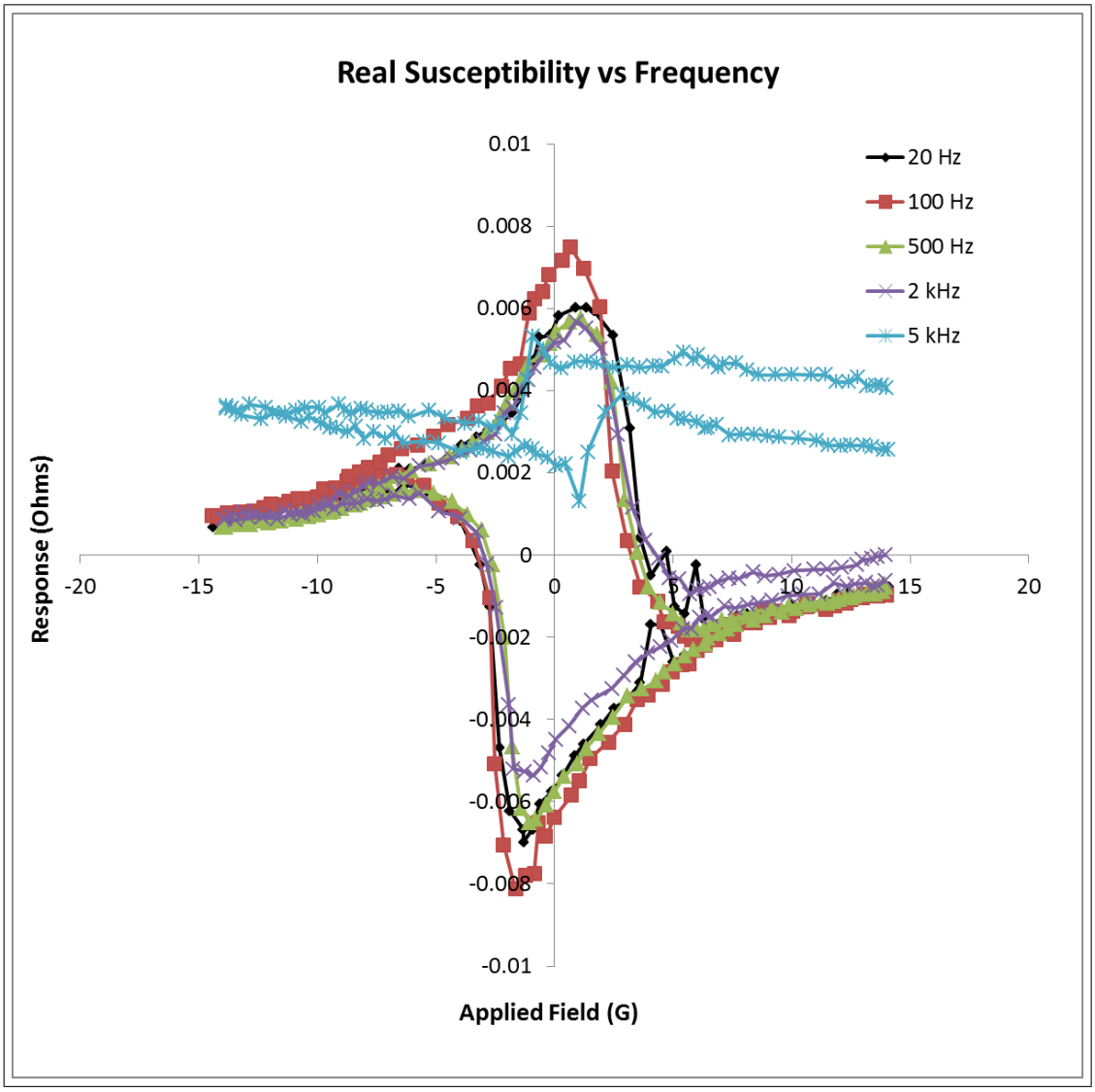

Figure 4.5: The real part of $\chi(H_{DC})$ for different frequencies. Runs at 50 Hz, 200 Hz, and 1 kHz were taken but are not shown to avoid cluttering the figure. The two peaks at positive and negative H are evident at low frequencies but move to $H = 0$ at high frequencies as magnetic hysteresis effects become less significant. Since the imaginary part dominates the real part of the susceptibility at high frequencies, the data at 5 kHz does not follow the shape of the data at lower f.

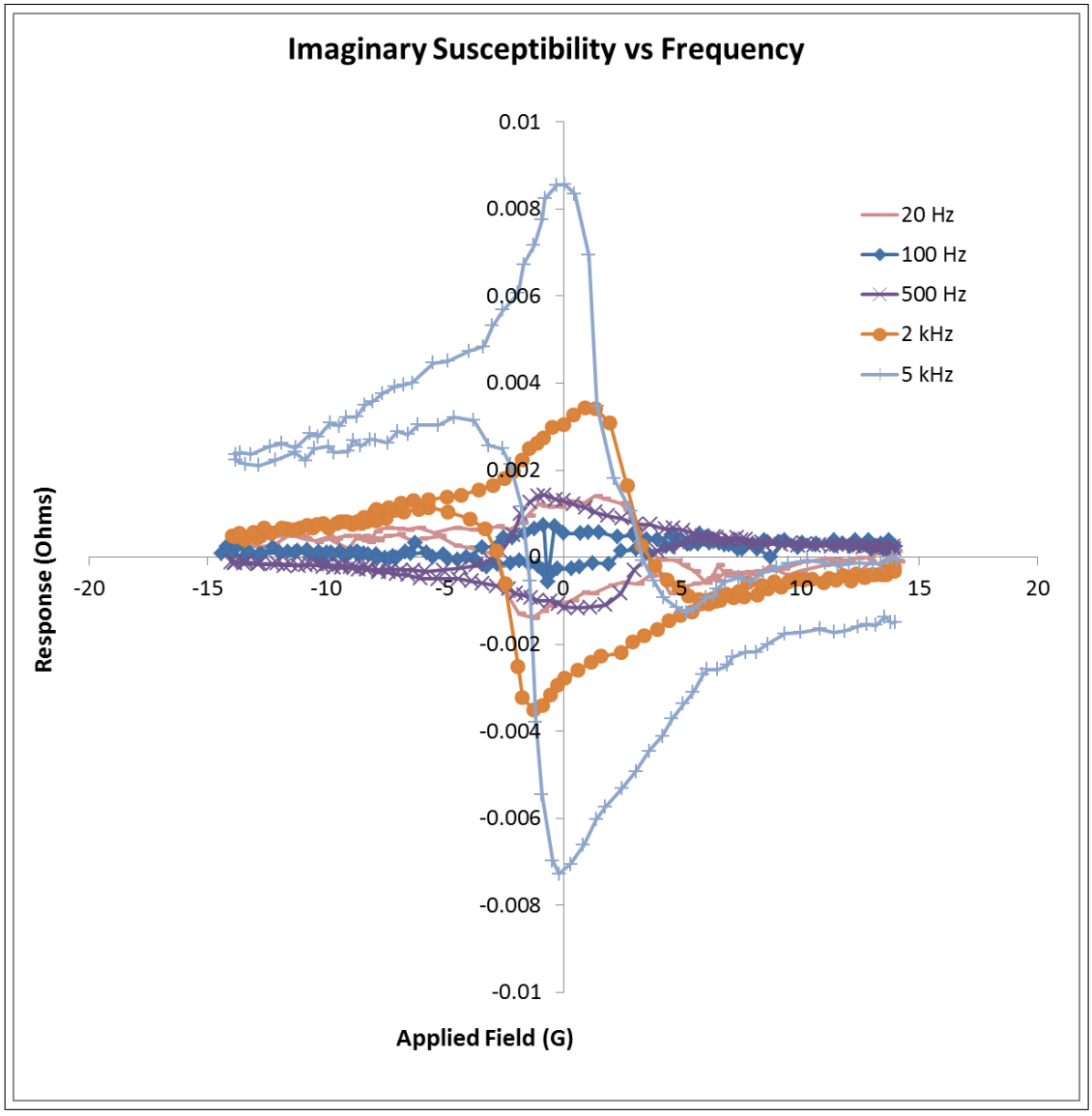

Figure 4.6: The imaginary part of $\chi(H_{DC})$ for different frequencies. The difference between the positive and negative values of $Im(\chi(H_{DC}))$ was determined and then plotted as a function of frequency to form Fig 4.8

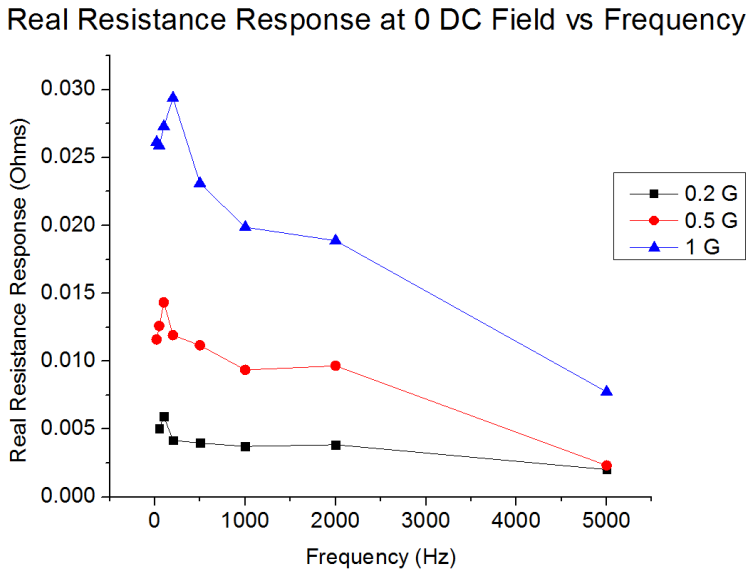

Figure 4.7: The difference between the two values of $Re(\chi(H_{DC} = 0))$ as a function of frequency from 20 Hz to 5 kHz, for $H_{AC} = 0.2$ G, 0.5 G and 1 G. Different AC amplitudes were chosen to find the optimum balance between large signal size for large H_{AC} and best linear response for small H_{AC}.

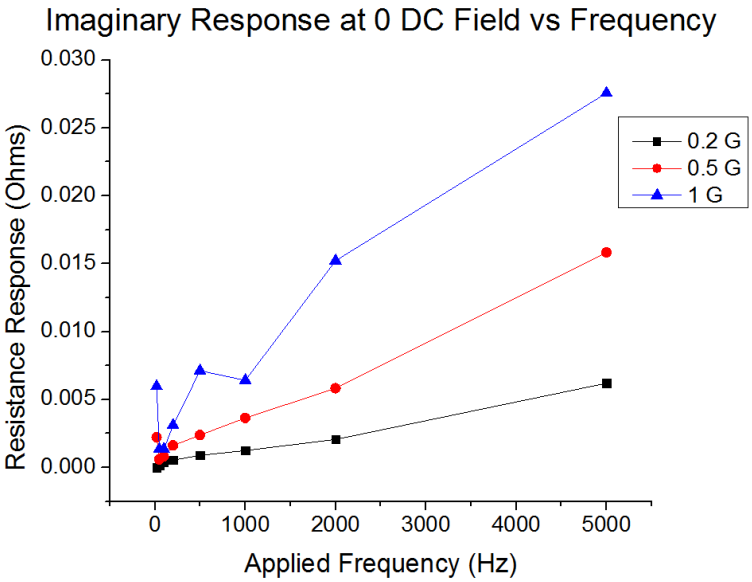

Figure 4.8: The difference between the two values of $Im(\chi(H_{DC} = 0))$ as a function of frequency from 20 Hz to 5 kHz, for $H_{AC} = 0.2$ G, 0.5 G and 1 G.

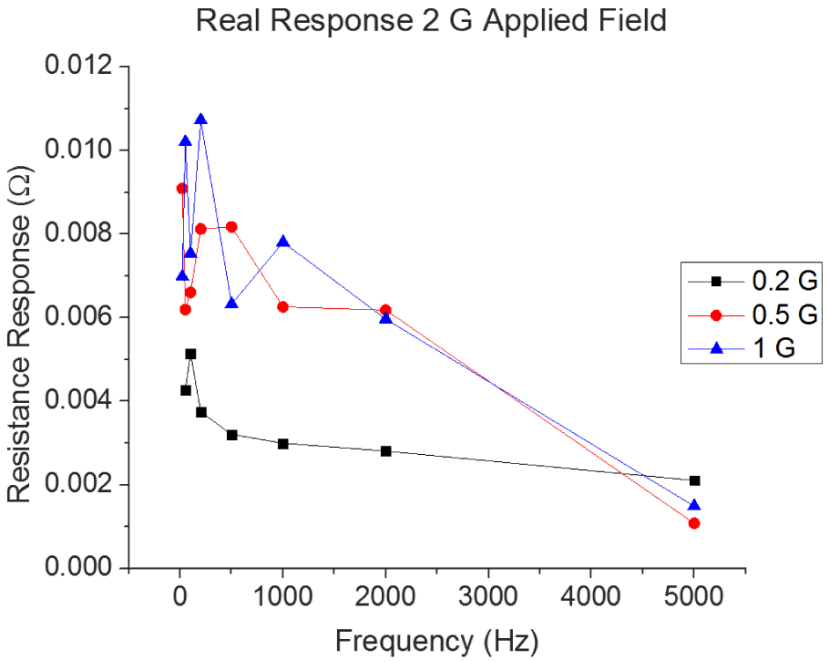

Figure 4.9: Taken from the same data set as Fig 4.7 except that each point now represents the difference between the two values of $Re(\chi(f))$ at $H_{DC} = 2.5G$ instead of $Re(\chi(f)$ at $H_{DC} = 0G$. Qualitatively the results are similar to Fig 4.7, except that the data appears more noisy.

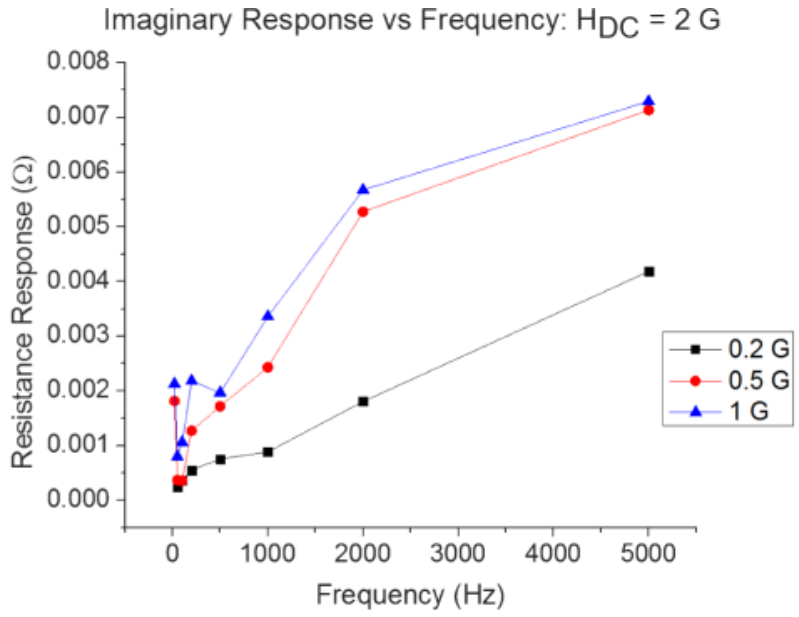

Figure 4.10: $Im(\chi(f))$ at $H_{DC} = 2.5G$ from 20 Hz to 5 kHz.

Chapter 5

Analysis and Implications for Magnetic Noise

5.1 Comparison to a Simple Harmonic Oscillator Model

Starting with the damped simple harmonic oscillator with a sinusoidal driving force

$$m\ddot{x} + \gamma\dot{x} + kx = F_0 \sin \omega t, \tag{5.1}$$

taking the Fourier transform and solving for the susceptibility yields

$$\chi = \frac{x}{F} = \frac{(\omega_0^2 - \omega^2) - i\beta\omega}{m((\omega_0^2 - \omega^2)^2 + \beta^2\omega^2)}. \tag{5.2}$$

Using the Kittel formula [16], the resonant frequency for this system is on the order of 1 GHz, so a low-frequency approximation applies. In this limit,

$$Re(\chi) \propto \frac{1}{\omega^2/\omega_0^2}, \tag{5.3}$$

$$Im(\chi) \propto \frac{\omega}{\omega_0} \tag{5.4}$$

The data at 0 G DC are replotted as log-log plots for clearer comparison to the SHO prediction in Fig 5.1 and Fig 5.2. In logarithmic form, the SHO model predicts that $Re(\chi(f))$ and $Im(\chi(f))$ should be linear with slopes of -2 and -1 respectively.

Performing least-squares fitting, the slopes of the imaginary log-log plots at 0.2 G, 0.5 G, and 1 G are 0.69, 0.68, and 0.69, and the slopes of the real curves are -0.18, -0.22, and -0.18, respectively. Neither component quantitatively matches the predictions of the SHO model, but the discrepancy in the real part is significantly greater than in

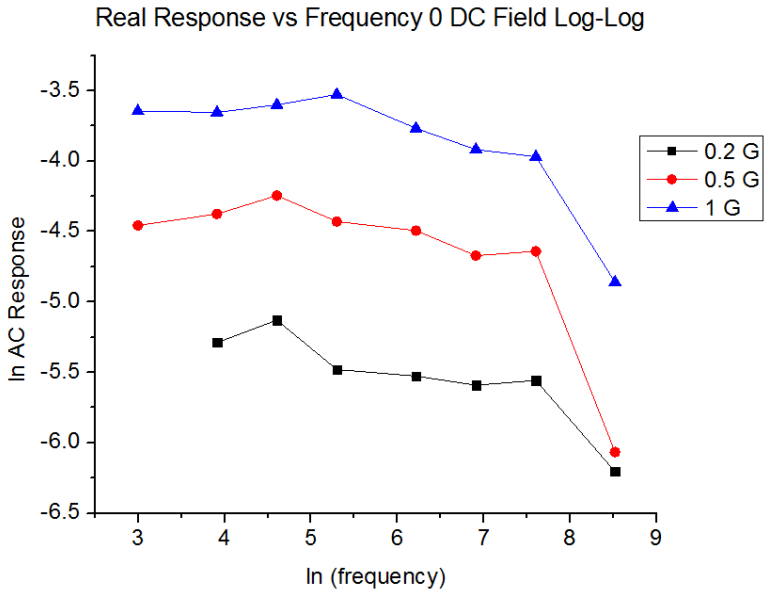

Figure 5.1: The data in Fig 4.7, redrawn as a log-log plot for clearer analysis. Modeling the magnetic domains as a driven damped simple harmonic oscillator predicts that $Re(\chi(f)) \propto 1/f^2$, so the curve would be linear with a slope of -2. The average slope of the curve is about -0.2, so the real component does not fit the SHO model.

the imaginary part. This discrepancy may reflect additional resistance effects in the sample contributing to the real response or also an inadequacy of the simple harmonic oscillator model. The SHO model involves a dissipative force giving rise to an imaginary susceptibility, but also a restoring force, and there may be no restoring force in this system.

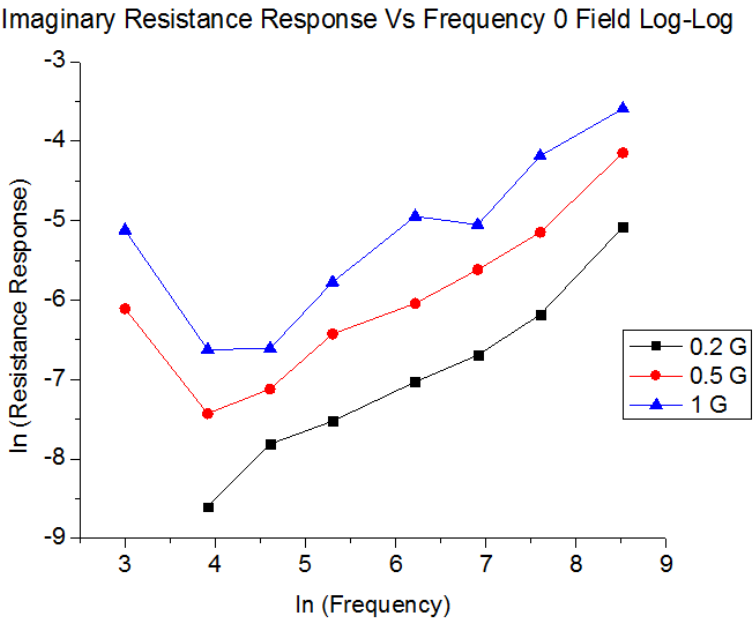

Figure 5.2: A log-log plot of Fig 4.8. The anomalously large value of susceptibility at 20 Hz is consistent across all measurements. Its origin is unknown, and when fitting to a line the data points at 20 Hz were ignored. The SHO predicts that $Im(\chi(f)) \propto f$, in which case the curve would be linear with slope 1. A linear fit yields an average slope of 0.69.

Chapter 6

Conclusion and Next Steps

In this experiment the AC magnetic susceptibility χ of a permalloy thin film was measured as a function of applied DC field, applied AC field magnitude and AC frequency. Anisotropic magnetoresistance was used to relate the magnetization to resistance, which provided the benefit of a simple physical system and the disadvantage of a small signal compared to previous measurements using giant magnetoresistance in magnetic tunnel junctions. The results were used to test applicability of the fluctuation-dissipation theorem in microscopic ferromagnetic systems and to predict the functional form of magnetic noise.

χ was measured first at $H_{DC} = 0$ as a function of H_{AC} to experimentally test the linear response necessary for application of FD. At AC amplitudes from 0.2 G to 1 G the response was found to be linear within 5%. χ was then measured as a function of f over the entire hysteresis loop at three different AC amplitudes. The imaginary part, $\chi''(f)$, was found to be very roughly linear with frequency, inconsistent with $1/f$ noise measurements but consistent with previous white noise measurements as well as a simple model of the magnetic domains in an AC field as a damped driven simple harmonic oscillator. The real part $\chi'(f)$ approximately varied as $f^{-0.2}$, inconsistent with the SHO prediction that $\chi'(f)$ should vary as f^{-2}.

Further work on this experiment would investigate in more detail the frequency dependence of χ', looking for extraneous contributions to the signal as well as extensions to the SHO model. In particular, the SHO model involves a restoring force or spring constant, and it is possible that there is no analogous restoring force on domains in an AC magnetic field and that the domains simply dissipate energy. This hypothesis could be tested by measuring the AC susceptibility over higher frequencies. The SHO model predicts a maximum real part at a resonant frequency, in which case the real susceptibility would be zero. However, the resonant frequency of 1 GHz may not be

practical in this experiment due to the large amount of current required to overcome the inductive impedance of the coils at high frequencies. AC susceptibility measurements should be performed on more permalloy samples to control for defects in the permalloy layer, which may pin the magnetization and lead to anomalies in the susceptibility. The experiment could also be repeated on GMR layers as in [6].

References

[1] S. Ikeda et al. Magnetic tunnel junctions for spintronic memories and beyond. *IEEE Transactions on Electron Devices*, 54:991–1002, 2007.

[2] A. Ozbay et al. Low frequency magnetoresistive noise in spin-valve structures. *Appl. Phys. Lett.*, 94:202506 1–3, 2009.

[3] O.V. Snigiriev, K.E. Andreev, and A.M. Tishin. Magnetic properties of thin ni films measured by a dc squid-based magnetic microscope. *Phys. Rev. B*, 55:14 429–14 433, 1997.

[4] Yuasa et al. Giant room-temperature magnetoresistance in single-crystal fe/mgo/fe magnetic tunnel junctions. *Nature Materials*, 3:868–871, 2004.

[5] R. Martin. Noise power spectral density estimation based on optimal smoothing and minimum statistics. *IEEE Transactions on Speech and Audio Processing*, 9:504–512, 2001.

[6] S.S.P. Parkin et al. Fluctuation-dissipation relation for giant magnetoresistive $1/f$ noise. *Phys. Rev. B*, 48:156–159, 1993.

[7] N. Smith and P. Arnett. White-noise magnetization fluctuations in magnetoresistive heads. *Appl. Phys. Lett.*, 78:1448–1450, 2001.

[8] F. Guo, G. McKusky, and E.D. Dahlberg. An investigation of the magnetic state dependent low frequency magnetic noise in magnetic tunnel junctions. *Appl. Phys. Lett.*, 95:062512 1–3, 2009.

[9] R. Kubo. The fluctuation-dissipation theorem. *Rep. Prog. Phys.*, 29:255–284, 1966.

[10] A. Zangwill. *Modern Electrodynamics*. Cambridge University Press, 2013.

[11] D. Griffiths. *Introduction to Electrodynamics*. Addison-Wesley, 4th edition, 2012.

[12] C. Kittel. On the theory of ferromagnetic resonance absorption. *Physical Review*, 73:155–161, 1948.

[13] Nahrwold et al. Structural, magnetic, and transport properties of permalloy for spintronic experiments. *Journal of Applied Physics*, 108:013907 1–6, 2010.

[14] B.D. Cullity and C.D. Graham. *Introduction to Magnetic Materials*. Wiley, 2009.

[15] T.R. McGuire and R.I.Potter. Anistropic magnetoresistance in ferromagnetic 3d alloys. *IEEE Transactions on Magnetics*, MAG-11:1018–1038, 1979.

[16] C. Kittel. *Introduction to Solid State Physics*. Wiley, 8th edition, 2004.

[17] Z.Q. Lei et al. Review of noise sources in magnetic tunnel junction sensors. *IEEE Transactions on Magnetics*, 47:602–611, 2011.

[18] P. Horowitz and W. Hill. *The Art of Electronics*. Cambridge University Press, 2 edition, 1989.

[19] R. O'Handley. *Modern Magnetic Materials: Principles and Applications*. Wiley, 2000.